



Band gap determination in multi-band-gap CuFeO_2 delafossite epitaxial thin film by photoconductivity

S. Vojkovic¹ · J. Fernandez¹ · S. Elgueta¹ · F. E. Vega¹ · S. D. Rojas¹ · R. A. Wheatley¹ · B. Seifert¹ · S. Wallentowitz¹ · A. L. Cabrera¹

© Springer Nature Switzerland AG 2019

Abstract

The photoconductivity within a wavelength range of 450–1100 nm was determined for a sample of epitaxial delafossite CuFeO_2 film grown by pulsed laser deposition. The film thickness was estimated to be 75 nm. The resistance of the films was determined with four-contact van der Pauw's method and using monochromatic illumination of the film. The most significant change in resistance resulted in three rapid lineal conductivity increases at photon energies of ~ 1.5 eV (gap-1), ~ 2.1 eV (gap-2) and ~ 2.5 eV (gap-3). The conductivity properties are well correlated with prior optical absorption results obtained in the NIR-VIS region using transmittance spectroscopy.

Keywords Semiconductor band-gap · Photoconductivity · Water photolysis · Thin film · Solar spectrum · Monochromatic light

1 Introduction

The global population has increased almost eighth-fold in the last 200 years. Consequently the demand for energy has also increased exponentially. Between the years 2005 and 2030 the demand for energy will increase by 55% the energy used at the beginning of that period of time [1]. Most of the energy being used now comes from fossil fuels but the problems related to burning fossil fuels are a driving motor to search for new renewable energy sources [2].

The combustion of fossil fuels yields emissions of gases such as carbon dioxide and methane which are responsible for the “greenhouse effect” in our planet and consequently the undesirable global warming.

Hydrogen is an attractive renewable energy source and seems to be a good alternative to energy obtained from fossil fuels combustion [3–5]. Hydrogen can be obtained from water electrolysis and in order to make this process more energetically efficient, the possibility of using solar

radiation in a photo-catalytic molecular decomposition of water is desirable and requires a multidisciplinary study.

Water dissociation by electrochemical photolysis was pioneered by Fujishima and Honda [6] using TiO_2 photo-electrodes.

Other widely reported electrode materials used for water splitting were WO_3 , CdS and other varieties of multi-component compounds [7, 8] which were broadly reviewed by Maeda [9]. However, research continues on chemically stable materials with a band gap greater than the water splitting potential of 1.23 V. Such materials should also display strong band to band absorption characteristics corresponding to peak solar irradiance. It has been predicted that such materials would enhance the efficiency of the photo-catalytic water decomposition [10].

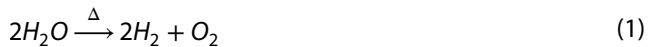
Sivula and Van de Krol [11] drew a diagram of several semiconducting materials and their band gap (valence and conduction edge) overlapping with the oxidation and reduction potential for water dissociation. The oxidation (production of O_2) and reduction (production of H_2)

✉ A. L. Cabrera, acabrera@fis.puc.cl | ¹Instituto de Física, Pontificia Universidad Católica de Chile, Av. Vicuña Mackenna 4860, Macul, Santiago, Chile.



potentials move according to the electrolyte used in the water. The most appropriate materials for photolysis are those whose valence and conduction edge (separated by band gap) fit within these two values of potential which are distant 1.23 V from each other.

The value of 1.23 V comes from thermodynamics equilibrium for the following chemical reaction:



The non-catalyzed chemical reaction needs 1.23 eV to break each O–H bond on the left side of the equation (there are four O–H bonds).

Therefore, this value of 1.23 V for the potentials separation is only an estimate since the dissociation of water is catalyzed by the surface of the photoconductor.

Several materials shown in Sivula and Van de Krol [11] diagram draw special attention: TiO₂ is the first semiconductor tested in water photolysis; CuFeO₂ with delafossite crystal structure; and a BiVO₄, recently reviewed [12], indicates that these materials have a lot of potential for photolysis.

One promising type of materials for these applications is CuFeO₂ and the whole family of oxides with a delafossite crystal structure. These compounds are characterized by the general chemical formula ABO₂, where A is a monovalent cation and B is a trivalent metal, any from Al to La [13]. This oxide family also displays multi-band-gap semiconductor behavior with energy gaps ranging between 1.1 and 3.6 eV and shows band-to-band absorption characteristics in response to illumination by UV, visible, and near infrared light. One advantage over the most common semiconductor materials is that the band gap(s) of delafossite oxides can be adjusted by changing the composition of the oxide. An additional advantage of these complex oxides is the abundance of the elements used in their composition such as Cu, Fe, Al, etc.

The CuFeO₂ delafossite oxide is known to be a p-type semiconductor [13]. However, reports of the fundamental energy gap vary widely. There are reports of multiple dominant absorption edges forming step-like patterns in the optical spectra of delafossite CuFeO₂ which are thought to emerge from the superposing of CuO₂ and Fe₂O₃ absorbance properties within the composition of delafossite CuFeO₂ [14]. Additionally, the breaking up of dipole-forbidden transition mechanisms is thought to emerge from Fe-3d states positioned within the forbidden regions of the crystalline structure [15].

Band gap measurements of CuFeO₂ samples have yielded scattered results within a wide range of energy. The difference in the band gap values could be explained by the fact that samples synthesis methods are all different: Pulsed Laser Deposition; sol–gel method; and solid

state reaction. Additionally, the material itself could be a multiple-band gap semiconductor.

The band gap results for CuFeO₂ have displayed strong absorption edges determined in the near infrared region ~ 1.2 eV [16–21]; absorption in the mid-visible region ~ 2.0 eV [22–26]; and absorption in higher energy, from blue to ultraviolet region ~ 3.0 eV [27–34]. Several groups have also reported multi-band gap results [22, 23, 25, 26].

In terms of more complex delafossite oxides, there are reports which describe the growth and characterization of B-site substitution in the oxide such as Cr for Fe in CuFe_{1-x}Cr_xO₂ [34]; substitution of Ni for Cr in CuCr_{1-x}Ni_xO₂ [35]; substitution of Mg for Cr in CuCr_{1-x}Mg_xO₂ [36]; and substitution of Fe for Ga in CuGa_{1-x}Fe_xO₂ [37]. All these substitutions displaced the energy of the band gaps.

In the last case [37], the substitution of 15% Fe in CuGaO₂ results in a band gap shifting from 2.55 eV down to 1.5 eV in the case of CuGa_{0.85}Fe_{0.15}O₂. A second band gap measured at 3.75 eV in CuGaO₂ remained in CuGa_{0.85}Fe_{0.15}O₂. In spite that one band gap was shifted for the substitutional alloy, the photochemical reduction of CO₂ to CO and CH₄ is active at wavelengths of 320 nm (3.8 eV) in both cases showing that the band gap at 1.5 eV was not relevant for this reaction.

In terms of photo-catalytic experiments there are recent reports of successful photo-catalytic water-splitting using CuGaO₂ electrodes. The CuGaO₂ material has shown favorable attributes in terms of its ability to catalyze overall water-splitting of adsorbed H₂O, meaning that its band edges are likely to be located at suitable energies in order to satisfy the conditions for H₂O redox potential. However, Lee et al. [38] also describe reduced photocatalytic activity below UV wavelengths (hν < 3.2 eV), in spite of the fact that CuGaO₂ having also shown weaker absorption edges around 2.7 eV in separate studies [37].

From this standpoint and with respect to the development of CuFeO₂—based delafossite materials for water dissociation electrodes, it is desirable to determine the active band gap for efficient photo-catalysis in multiple band gap materials. This requires developing new testing techniques in addition to optical techniques which are the most common used in the literature.

In the present work we measured the conductivity of a CuFeO₂ thin film when exposed to light as a function of wavelength to correlate conductivity with the optical characteristics of the sample. Since the catalytic activity of the electrode material depends on the number of holes generated by the light in the semiconductor and the number of holes able to arrive to the surface of the semiconductor (electrode), knowledge of photoconductivity properties of the material is crucial. We measured the film conductivity using van der Pauw four-contact method while illuminated with a narrow light wavelength which is obtained

from a halogen lamp passing through a monochromator. The photoconductivity method is validated using a CdS film with a well determined band gap.

The high quality epitaxial nature of our CuFeO₂ thin film samples was previously confirmed by TEM, XRD and Raman spectroscopy.

2 Experimental methods

2.1 Sample description

CuFeO₂ (001) films were deposited onto Al₂O₃ (001) substrates from a stoichiometric polycrystalline CuFeO₂ target using pulsed laser deposition. Details of the experimental setup and procedure have been described elsewhere [21]. The film was grown in a vacuum system at 600 °C under an O₂ partial pressure of 1.33×10^{-2} Pa.

CdS films, 100 nm thick were sputtered deposited over a 1" × 1" quartz substrate and they were obtained from Matsurf Technologies Inc., St. Paul, Minnesota.

2.2 Sample characterization

2.2.1 Atomic force microscopy (AFM)

Atomic Force Microscopy (AFM) micrographs were measured using a commercial AFM NanoWizard 3 from JPK instruments. Scans of 10 × 10 μm and 1 × 1 μm were performed using tapping mode in different areas of the samples.

2.2.2 X-ray diffraction (XRD)

A four-axis Rigaku XRD system with a Cu rotating anode (CuKα radiation) and Huber goniometers was used for determining the crystal structure of the deposited films. CuFeO₂ and CuFe₂O₄ phases were identified using powder diffraction files no. 01-075-2146 and no. 00-025-0283, respectively.

2.2.3 Raman spectroscopy

Raman spectra were obtained using a LabRam010 system from Instruments S.A. (Horiba), featuring a 5.5 mW He–Ne laser (632.8 nm wavelength). This instrument used an Olympus confocal optical microscope with a light spectrometer in a back-scattering geometry where the incident beam was linearly polarized and spectral detection was non-polarized. The spectra were taken at room-temperature using a × 100 objective (~ 10 μm spot size) with an energy resolution of approximately 1 cm⁻¹.

2.3 Optical measurements

A visible/NIR transmittance and reflectance spectroscopy system was set up to measure the optical response of the samples. The apparatus previously described [23] uses a 9 W tungsten-halogen model SL201 from Thorlabs. The light sources provide a broadband spectrum. The white light goes through a monochromator (Triax 180, Jobin–Yvon–Horiba) equipped with a 1200 g/mm blazed ruled grating and set up to provide near monochromatic light within a 1 nm wavelength resolution. Silicon UV enhanced photodetector are used to collect transmitted and reflected light (angle of transmittance is recorded at normal incidence ($\theta = 0^\circ$) while angle of reflectance is recorded at $\theta < 10^\circ$). The white light beam is chopped (730 Hz) before entering the monochromator and the signals are measured using lock-in amplifiers. All data is normalized to the halogen lamp spectrum.

2.4 Electrical conductivity measurements

Four metallic contacts were placed on the film. To make sure that the contacts adhered well to the surface of the CuFeO₂ film a 5 nm Pt layer was e-beam evaporated followed by a 30 nm Au layer deposited via physical vapor deposition. Then, silver paint was used to attach four thin cables on top of Au contacts. The CuFeO₂ film was placed in a manipulator of a high vacuum system and the four electrical contacts spot-welded to an electrical feed-through. The sample was fixed over a Macor insulating substrate using isolated stainless steel mini clamps. The sample temperature was measured with K-type thermocouple using a Fluke multimeter. The sample inside the vacuum system was facing a quartz window transparent to UV/visible/NIR light.

The electrical resistance of the sample is determined with van der Pauw [41] technique (four-point method). The current and voltages are obtained and measured with Radiant RT66-B (Ferrodevices) modified since our sample is passive and not active such as a ferroelectric film. A schematic configuration of the circuit is shown in Fig. 1. The van der Pauw method requires exchange positions between the two contacts where voltage is applied and the two contacts for sensing the current. Our results were obtained with 4 configurations and the respective reciprocal connections did not change more than 0.01%, indicating high quality electrical contacts made with the silver paint.

The monochromator used in the optical measurements equipped with the same 1200 g/mm blazed ruled grating and a broadband light from a Thorlabs SL201 (VIS-IR) is used to shine light over the CuFeO₂ film while measuring its conductivity. The light wavelength is selected when passing through a wide adjustable slit in

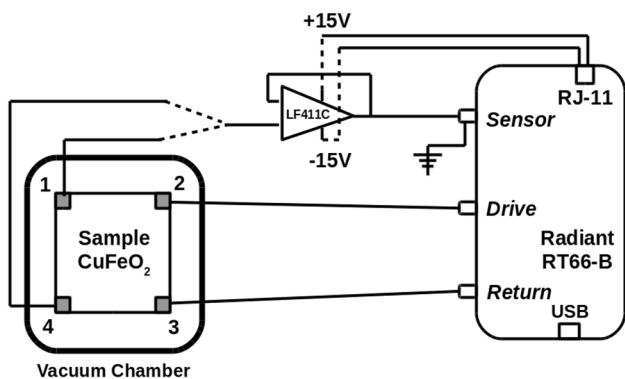
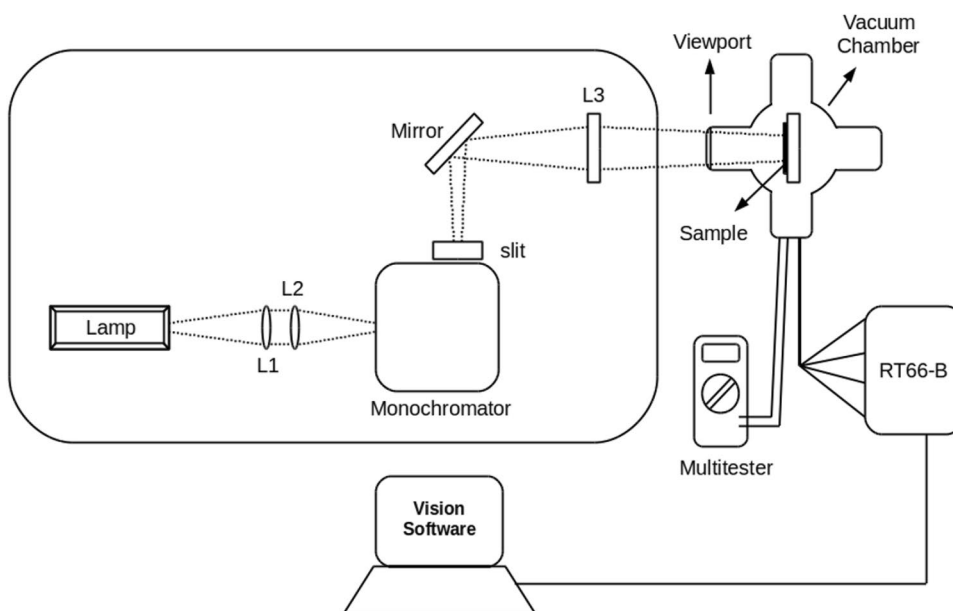


Fig. 1 Schematic diagram of four-contact circuit for resistance measurement using van der Pauw's method

inverse configuration (Edmund Optics) which provides a narrow wavelength resolution (~ 2 nm). The light spot is then deviated by an optical mirror at 45° and focused onto the CuFeO₂ thin film sample through viewport of the high-vacuum chamber using a condenser lens (focal length F = 125 mm./50.8 mm diameter—Thorlabs).

Electrical resistance measurements were made after the sample was exposed to a fixed wavelength for 20 min, taking 8 min to collect the data. Care was taken to eliminate any source of external light while the selected wavelength entered the vacuum chamber through the quartz window. Electrical resistance measurements were made at ~ 25° C and total pressure of 1 × 10⁻⁶ Torr inside the vacuum chamber. The experimental setting combining light illumination and electrical conductivity measurement is shown in Fig. 2

Fig. 2 Schematic diagram of the optical apparatus: A 9 W tungsten halogen lamp is used as a broadband light source. The light goes through a monochromator and the selected wavelength is reflected by a mirror to the sample located inside a vacuum system. L₁, L₂, L₃ are optical lenses



3 Results

3.1 Structural and morphological characterization of CuFeO₂ film

An AFM image of the surfaces of the CuFeO₂ film (100 nm thickness) with scanning area of 10 × 10 μm is shown in Fig. 3a and scanning an area of 2 × 2 μm is shown in Fig. 3b. The surface of the samples appears very flat at 10 × 10 μm scale. Images obtained in areas of 2 × 2 μm show an array of agglomerated with sizes less than 10 nm in diameter.

XRD and Raman characterization and analyses of the CuFeO₂ films are described in detail elsewhere [21]. A summary of the results is: XRD spectra for CuFeO₂ film displayed only peaks corresponding to c-axis reflections and corresponding to Miller indexes (003), (006), (009) and (0012). A typical XRD spectrum of CuFeO₂ is shown in Fig. 4a. These oriented planes show the high quality epitaxial growth of CuFeO₂. Although the formation of CuFe₂O₄ spinel material within the thicker CuFeO₂ sample with small peaks corresponding to (222) oriented plane at 2θ = 54.6° and (333) oriented plane at 2θ = 85.7°, are visible.

Raman spectra were taken at room temperature using a 100× objective (~ 10 μm spot size) with an energy resolution of approximately 1 cm⁻¹. The CuFeO₂ film showed a typical delafossite Raman spectrum shown in Fig. 4b with three main peaks at 350, 511 and 689 cm⁻¹. The peak located at 350 cm⁻¹ was attributed to the E_g vibrational mode along the c-axis of the octahedral structure; the peak at 689 cm⁻¹ was attributed to the A_{1g} vibrational mode along a plane perpendicular to the c-axis; the peak

Fig. 3 AFM topography images for 75 nm thick CuFeO₂ epitaxial film **a** 10 × 10 μm scale, **b** 2 × 2 μm scale

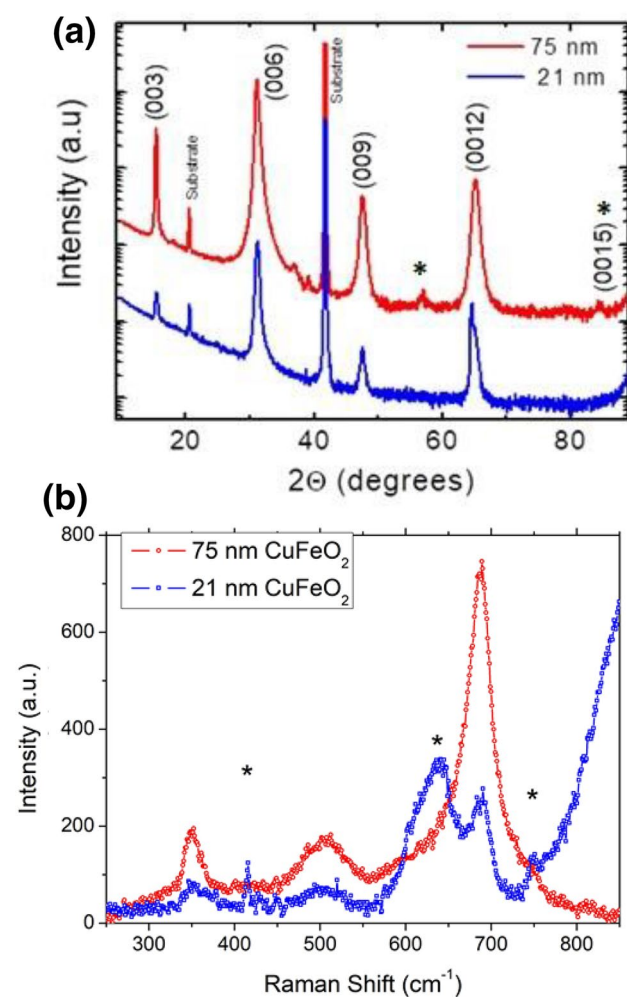
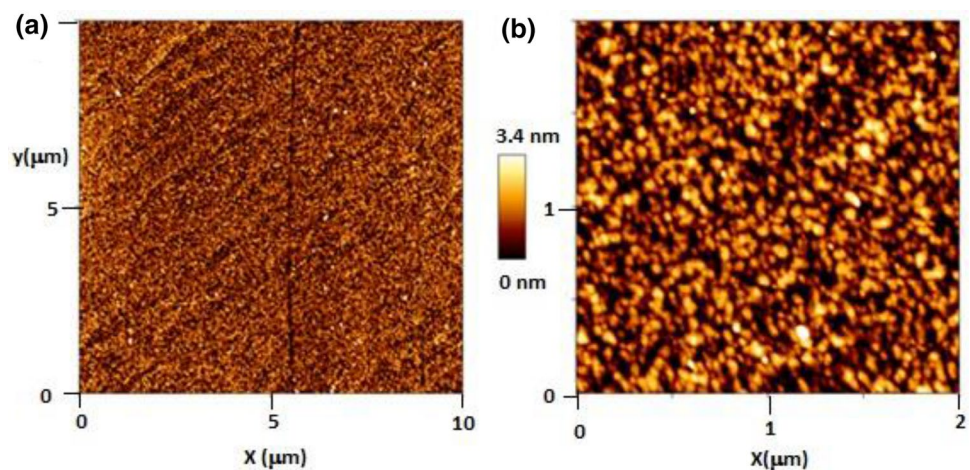


Fig. 4 **a** XRD diffraction patterns for both CuFeO₂ samples: 21 nm thick film is shown with a blue line; 75 nm thick film is shown with a red line. The cuprospinel phase is shown with the sign (*) **b** Raman spectra of the same samples: blue squares corresponds to the spectrum of 21 nm CuFeO₂ film, red circles corresponds to the spectrum of 75 nm CuFeO₂ film. Raman peaks labeled with (*) correspond to the Al₂O₃ substrate

at 511 cm⁻¹ was attributed to non-zero wave vector phonons typical of crystalline defects [39, 40].

3.2 Optical measurements

Transmittance spectra were recorded for a pure quartz substrate and a 100 nm CdS thin film on quartz substrate sample. The transmission spectra are displayed in Fig. 5a. Transmittance spectra were also recorded for the 75 nm CuFeO₂ film and displayed in Fig. 5b. The sample is very transparent and the transmission spectrum is amplified 35 times (35×). In the same plot we show the spectra of the halogen lamp and the light through a dydimum glass use to calibrate the monochromater using the typical absorption lines of didymium.

Tauc-gap analyses were performed on each spectrum in order to further relate spectral absorption edges with estimations of direct and indirect band to band transition energies and the band gap from which they emerged. The transmittance spectra results were then treated in order to determine the band gap energy (E_g) of each sample using Tauc's expression [42–44],

$$\alpha h\nu = b(h\nu - E_g)^n \quad (2)$$

In Eq. (2), h is Planck's constant, ν is the frequency of the incident light, α is the absorption coefficient, b is a proportional constant, and E_g is the band gap energy defined as the difference between the lowest energy level in conduction band and the highest energy level in the valence band. When linearity was identified within the Tauc plot, extrapolation to the x -axis revealed possible optical band gap energies for the sample. The plotting is repeated, once using power $n = 1/2$ so as to identify direct gap behavior and secondly using power $n = 2$ to identify characteristics of indirect energy gaps within the samples. For the CdS sample a Tauc plot with $n = 1/2$ was made and displayed

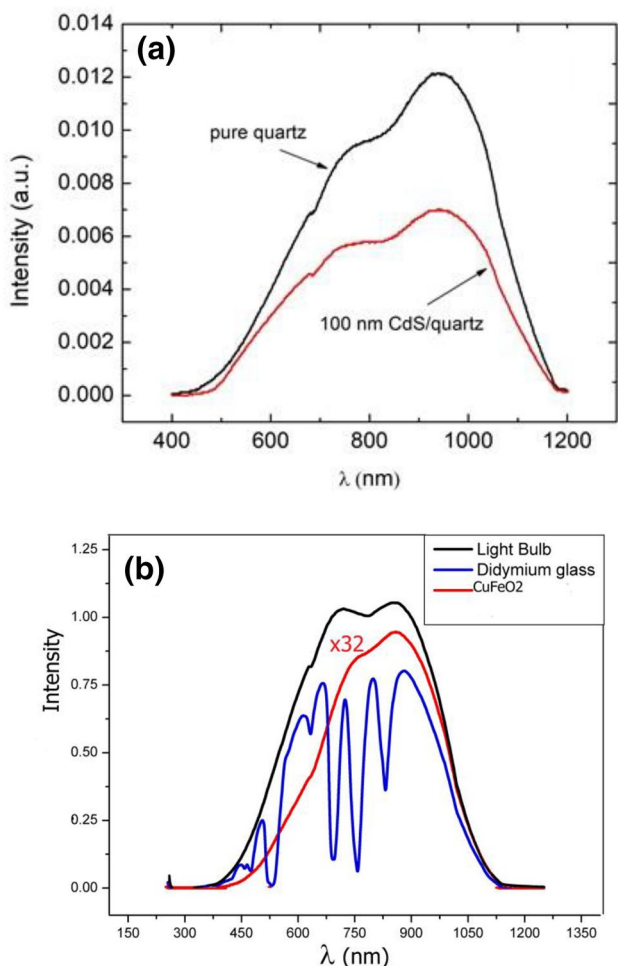


Fig. 5 **a** Plot of the transmittance spectra as a function of photon energy for the CdS sample: black line correspond to the spectrum of pure quartz substrate, red line corresponds to the spectrum of sample of 100 nm CdS film on quartz substrate. **b** Plot of the transmittance spectra $\times 35$ as a function of photon energy for the CuFeO₂ film. In the same plot it is shown the spectra of the halogen lamp and the spectra through a didymium glass filter used to calibrate the monochromator

in Fig. 6a. A band gap of 2.4 eV can be estimated from the intersection of the linear part of the plot with the energy scale at zero ordinate. This value is in perfect agreement with the well accepted value for CdS bulk semiconductor [46]. The Tauc plot for the 75 nm CuFeO₂ film is displayed in Fig. 6b. Linear regions extrapolating at zero ordinate indicate two direct transition band gaps: 1.2 and 2.2 eV. Very few data points are in the UV region in order to ascertain a third gap at 3.0 eV.

Transmittance spectra were also recorded for a 21 nm CuFeO₂ film (shown in Fig. 6b) and reported previously [23]. Both samples showed relatively stronger absorption in the NIR-(Red) region (in the range $1.0 \text{ eV} < h\nu < 1.5 \text{ eV}$) and in the Vis region ($1.8 \text{ eV} < h\nu < 2.9 \text{ eV}$). The change in

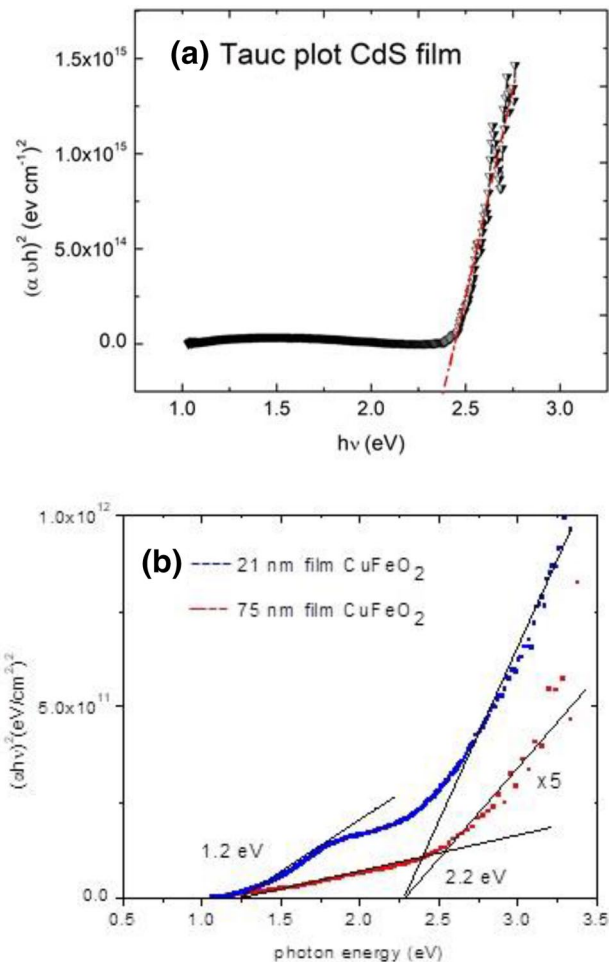


Fig. 6 **a** Tauc-plot from transmittance data [$n = 1/2$ in Eq. (2)] for the 100 nm CdS film. **b** Tauc-plot from transmittance data [$n = 1/2$ in Eq. (2)] for the 21 nm and 75 nm CuFeO₂ film

transmission is consistent with the variation in thickness and optical path of absorption.

The results for recorded energy gaps (pertaining to measurable absorption edges) for the two CuFeO₂ samples from both the transmittance and reflectance measurements are summarized in Table 1.

From transmittance measurements, the first fundamental Tauc-gap was measured at 1.3 eV for the range between 1.0 and 2.0 eV, is in fair agreement with those reported in Refs. [16–21]. At higher energies, a secondary Tauc-gap

Table 1 Summary of all measurable absorption edges and corresponding estimated Tauc-energy gaps

Sample	Tauc-gap 1 (direct transition) (eV)	Tauc-gap 2 (direct transition) (eV)
21 nm CuFeO ₂	1.3 ± 0.2	2.2 ± 0.2
75 nm CuFeO ₂	1.2 ± 0.2	2.2 ± 0.2

was observed at 2.2 eV (in agreement with [22–26]) and possibly a third absorption edge pertaining to ~ 3 eV.

With regard to the small amount of cuprospinel formed on the 75 nm CuFeO_2 film, Nawle et al. [47] reported a direct band gap of 1.95 eV for cuprospinel (CuFe_2O_4). The amount of cuprospinel in the 75 nm CuFeO_2 film is very small and it does not show up in the 21 nm CuFeO_2 film. Thus, cuprospinel does not affect the direct band gap of 2.2 eV measured in the CuFeO_2 films. Neither affects photoconductivity of the samples.

3.3 Conductivity measurements

3.3.1 CdS conductivity

Before electrical resistance measurements as a function of wavelength were made, two critical parameters were measured under the same conditions of vacuum and temperature. First, the electrical resistance of the sample was measured in complete darkness to obtain the highest resistance value, larger than 40 k Ω . A second value of the sample resistance was obtained under illumination broadband light using the zeroth order diffraction of the monochromator (20 k Ω). This means the white light travels along the same optical path of a selected given wavelength. Subsequently, electrical resistance was measured as a function of an incoming wavelength. The electrical resistance was measured at a given wavelength within the range 460–580 nm and light wavelength was change in discrete steps of 30 nm. The resistance of the film was decreased by a factor of two right at wavelength value identical to the band gap energy (2.4 eV) of CdS as displayed in Fig. 7a. The relative small change can be explained by the small light intensity in that range of wavelength. The phenomenon known as photoconductivity resulting in increased conductivity in a sample is not very pronounced at high temperatures except when the illumination is by an intense beam of light. At low temperatures, illumination results in excitation of localized carriers to conduction or valence band [48].

3.3.2 CuFeO_2 conductivity

The electrical resistance of the sample was measured in complete darkness to obtain the highest resistance value and a second value of the sample resistance was obtained under illumination broadband light using the zeroth order diffraction of the monochromator.

These values are summarized in Table 2.

The resistance difference appears insignificant but the value is consistent with the change in carriers observed in the same photoconductor (CuFeO_2 sol–gel made) [49] at 0.5 sun illumination ($0.5 \times 10^9 \text{ cm}^{-2} \text{ pulse}^{-1}$). This can be

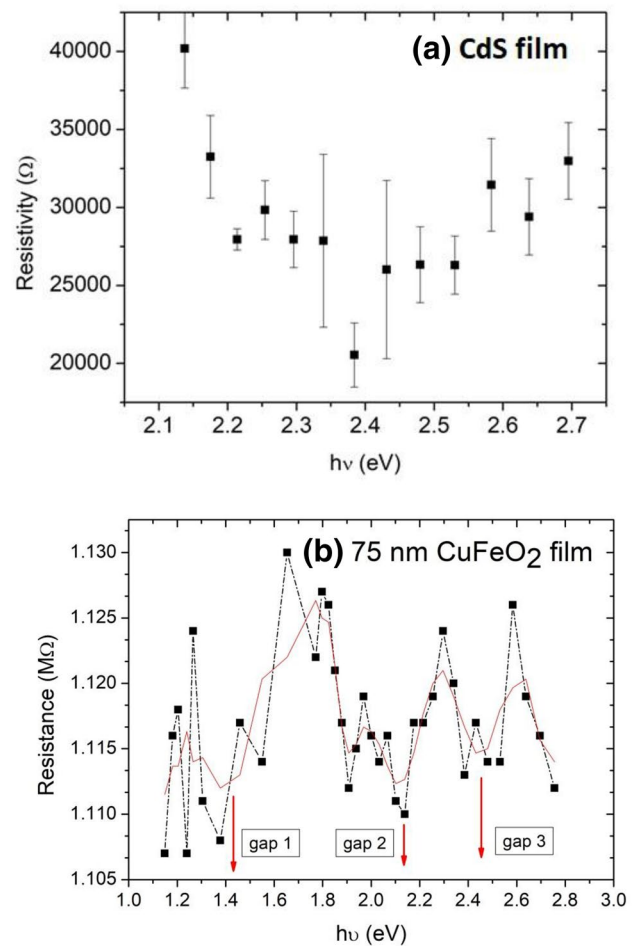


Fig. 7 **a** Plot of electrical resistance of 100 nm CdS film as function of radiation energy. **b** Plot of electrical resistance of 75 nm CuFeO_2 film as function of radiation energy

Table 2 Electrical resistance and resistivity of the sample of 75 nm thick CuFeO_2 in both extreme illumination conditions

Exposure condition	Electrical resistance (M Ω)	Resistivity (Ωm)
Complete darkness	1.132	8.49×10^{-2}
Zero order broadband light	1.117	–

‘–’ Not given because production of electron–hole pairs depends on the light power per area and it is not an intrinsic property of the film

explained by the results obtained for CdS and shown in Fig. 7a. The decrease of resistivity happened right at the photon energy corresponding to the band gap energy of the semiconductor. The excess of energy of photon with larger energy than that corresponding to the band gap is dissipated in heat, in other words, wasted.

Subsequently, electrical resistance was measured as a function of an incoming wavelength. The electrical

resistance was measured at a given wavelength within the range 450–1100 nm and light wavelength was change in discrete steps with an uncertainty of ± 5 nm.

These results are displayed in Fig. 7b. All the data obtained are of a lower value than the resistance obtained in darkness. The resistance obtained with white light (zero order) illumination is close to an average value. Local minimum related to the band gaps are obtained by fitting and average line (red) due to the high scatter in the data. The red line shows gap-1 at ~ 1.4 eV (886 nm), gap-2 at ~ 2.1 eV (591 nm) and gap-3 at ~ 2.5 eV (496 nm).

The resistance data should be normalized to light intensity at different wavelengths and corrected according the halogen lamp characteristics. The halogen lamp SL201L spectrum, intensity as a function of light energy, provides by Thorlabs is displayed in Fig. 8. The intensity of the lamp is large in the IR region a small in the UV region.

The light intensity was measured using a Si photodiode (with area $A = 0.3 \text{ cm}^2$) placed between condenser lens (L_3 in Fig. 2) and the quartz window of the vacuum chamber. The light intensity increases from 67 nW/cm^2 for 450 nm light up to 333 nW/cm^2 for 1100 nm light.

We calculated the change in resistance from the resistance measured in dark (R_0) using the following equation

$$\frac{\Delta R}{R_0} = \frac{R_0 - R}{R_0}, \tag{3}$$

The change in resistance was normalized by relative light intensity $I(\lambda)$, the fractional intensity at a given wavelength. A plot of $\left(\frac{\Delta R}{R_0}\right) / A \times I(\lambda)$ as a function of photon energy of the incoming light is shown in Fig. 9. The most significant

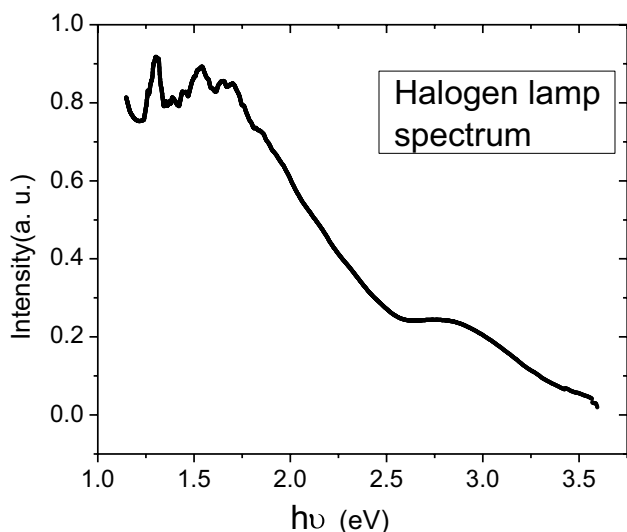


Fig. 8 Incident light spectrum corresponding to the halogen lamp SL201L from Thorlabs

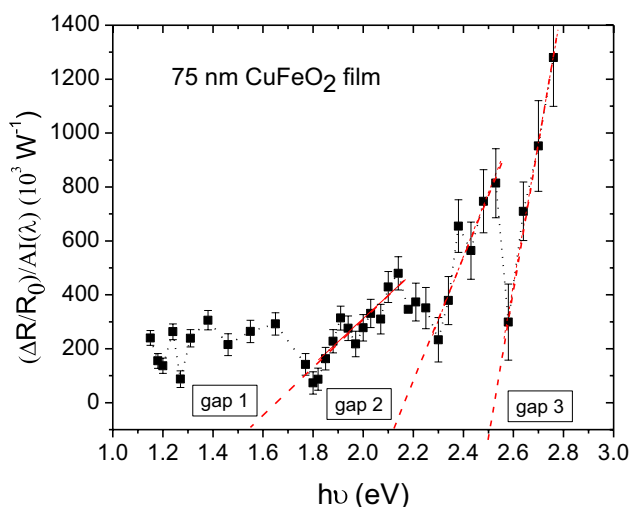


Fig. 9 Light intensity-normalized change of resistance $\left(\frac{R(\lambda)-R_0}{R_0}\right) / A \times I(\lambda)$ 75 nm CuFeO₂ film as a function of photon energy. R_0 is the resistance of the film in the dark and the units of light intensity-normalized change of resistance are 10^3 W^{-1}

change in resistance is a rapid linear increased which intersect the energy scale at gap-1 ~ 1.5 eV, gap-2 ~ 2.1 eV and gap-3 ~ 2.5 eV. These data rapid increase in this type of plots is related to increase in conductivity of the sample. Thus, the interpretation of Fig. 8 is that each time that the energy of the incoming light exceeds the energy gap of the semiconductor, the conductivity in the film increases. The bandgaps at 2.1 eV and 1.5 eV are in agreement with the value obtained from transmittance Tauc plots. But now we can ascertain the existence of a third gap at 2.5 eV which is in the near UV region. This experimental method of combining resistivity with radiation illumination in order to determine band gap of photo-conductors was validated using a thin film of CdS in which the fast increase in conductivity was determined at 2.40 ± 0.05 eV.

The absorption edges that we measured in the region of 1.0–1.3 eV can be compared and attributed to the expected 1.2–1.4 eV indirect L– Γ transitions in Ref. [24], with an expected Urbach tail formed from sub-gap indirect d–d state transitions. Both CuFeO₂ samples displayed the activation of a direct transition in the 2.0–2.2 eV region. This absorption edge can be attributed to the activation of direct L-point transitions and direct Γ -point transitions calculated to be at 1.6 eV and 2.4 eV respectively [24]. It is possible that the absorption observed in this spectral region takes place by a super positioning of direct transitions over both symmetry points. Each spectrum obtained also indicates the activation of a possible higher absorption edge located in the range $h\nu > 3.1$ eV. These effects are particularly prominent in the reflectance spectra [26] and such wide band-energy gaps have been reported before

[22]. These absorption edges are likely to result from valence band to second conduction band transitions or to absorption via channels located higher up within the conduction bands which are known to possess relatively large optical cross-sections. These higher energy absorption channels are thought to form an apparent optical edge. This explanation is explored in detail by Nie et al. [45].

4 Conclusions

The photoconductivity of a well characterized epitaxial thin film of CuFeO_2 was measured as a function of near monochromatic light selected from a W-halogen lamp through a monochromator. The film conductivity was obtained using van der Pauw four-contact method while illuminating the film. The conductivity shows mark jumps between 1.5 eV, 2.1 and 2.5 eV which are well correlated with the optical absorption results. Analysis of Tauc plot from optical data for the CuFeO_2 thin films showed predominant absorption edges at 1.2 ± 0.2 eV and 2.2 ± 0.2 eV. The higher energy gap at ~ 2.5 eV seen in resistance measurements was not clearly determined from optical transmittance due to the poor response of the Si diodes at UV wavelengths. The photoconductivity technique implemented to determined band-gaps for CuFeO_2 was validated by doing same measurement in a CdS film for which a bad gap of 2.4 eV was observed. Further investigations of the carrier mobility and photo-catalytic reactions on the sample surfaces will help determine the impact of the substituted layers and surface absorption channels on the generation of the electron-hole pairs required for photocatalytic processes within the materials investigated.

Acknowledgements Thanks are due to Dr. T. Joshi and Professor D. Lederman (UC, Santa Cruz) for providing the samples of CuFeO_2 films, grew by PLD at West Virginia University. This work was supported by FONDECYT Proyecto Anillo ACT1409 (Comisión Nacional de Investigación Científica y Tecnológica).

Compliance with ethical standards

Conflict of interest The authors declare that they have no conflict of interest.

References

- Reasons for increase in demand for energy, BBC online (2019) <https://www.bbc.com/bitesize/guides/zpmmmp3/revision/1>. Accessed 20 Nov 2018
- Angelis-Dimakisa A, Biberacherb M, Dominguez J, Fioreded G, Gadochab S, Gnansounouf E, Guarisod G, Kartalidisa A, Panichellif L, Pinedoc I, Robbag M (2011) Methods and tools to evaluate the availability of renewable energy sources. *Renew Sustain Energy Rev* 15(2):1182–1200
- Andrews John, Shabani Bahman (2012) Re-envisioning the role of hydrogen in a sustainable energy economy. *Int J Hydrog Energy* 37:1184
- Dresselhaus MS, Thomas IL (2011) Alternative energy technologies. *Nature* 414:332–337
- Lao SJ, Qin HY, Ye LQ, Liu BH, Li ZP (2010) A development of direct hydrazine/hydrogen peroxide fuel cell. *J Power Sources* 195(13):4135–4138
- Fujishima A, Honda K (1972) Electrochemical photolysis of water at a semiconductor electrode. *Nature* 238(5385):37–38
- Finlayson AP, Tsaneva VN, Lyons L, Clark M, Glowacki BA (2016) Evaluation of Bi-W-oxides for visible light photocatalysis. *Phys Status Solidi A* 203(2):327–335
- Gratzel Michael (2001) Photoelectrochemical cells. *Nature* 414:338–344
- Maeda K (2011) Photocatalytic water splitting using semiconductor particles: history and recent developments. *J Photochem Photobiol C: Photochem Rev* 12(4):237–268
- Shockley W, Quiesser HJ (1961) Detailed balance limit of efficiency of p-n junction solar cells. *J Appl Phys* 32(3):510–519
- Sivula K, Van de Krol R (2016) Semiconducting materials for photoelectrochemical energy conversion. *Nat Rev Mater* 2016:15010
- Abdi FF, Berglund S (2017) Recent development in complex metal oxide photoelectrodes. *J Phys D Appl Phys* 50:193002
- Huda MN, Yan Y, Walsh A, Wei S-H, Al-Jassim MM (2009) Group-III A versus III B delafossites: electronic structure study. *Phys Rev B* 80:035205
- Galakhov VR, Poteryaev AI, Kurmaev EZ, Anisimov VI, Bartkowski St, Neumann M, Lu ZW, Klein BM, Zhao Tong-Rong (1997) Valence-band spectra and electronic structure of CuFeO_2 . *Phys Rev B* 56:4584–4591
- Hiraga H, Makino T, Fukumura T, Weng H, Kawasaki M (2011) Electronic structure of the delafossite-type CuMO_2 (M = Sc, Cr, Mn, Fe, and Co): optical absorption measurements and first-principles calculations. *Phys Rev B* 84:041411(R)
- Tablero Crespo C (2018) Potentiality of CuFeO_2 -delafossite as a solar energy converter. *Sol Energy* 163:162–166
- Pavunny S, Kumar A, Katiyar RS (2010) Raman spectroscopy and field emission characterization of delafossite CuFeO_2 . *J Appl Phys* 107:013522
- Omeiri et al (2009) Electrochemical and photoelectrochemical characterization of CuFeO_2 single crystal. *J Solid State Electrochem* 13:1395–1401
- Barot N et al (2017) Structure, I-V characteristics and optical studies of delafossite CuFeO_2 and $\text{CuFe}_{0.96}\text{Ti}_{0.03}\text{V}_{0.01}\text{O}_2$ prepared under high vacuum. In: AIP conference proceedings, vol 1837, p 040031
- Read Carrie G, Park Y, Choi K (2012) Electrochemical synthesis of p-type CuFeO_2 electrodes for use in a photoelectrochemical cell. *J Phys Chem Lett* 3:1872–1876
- Joshi Toyanath, Senty Tess R, Trappen Robbyn, Zhou Jinling, Chen Song, Ferrari Piero, Borisov Pavel, Song Xueyan, Holcomb Mikel B, Bristow Alan D, Cabrera Alejandro L, Lederman David (2015) Structural and magnetic properties of epitaxial delafossite CuFeO_2 thin films grown by pulsed laser deposition. *J Appl Phys* 117:013908
- Benko FA, Koffyberg FP (1987) Opto-electronic properties of p- and n-type delafossite, CuFeO_2 . *J Phys Chem Solids* 48:431–434
- Wheatley RA et al (2017) Comparative study of the structural and optical properties of epitaxial CuFeO_2 and $\text{CuFe}_{1-x}\text{Ga}_x\text{O}_2$

- delafossite thin films grown by pulsed laser deposition methods. *Thin Solid Films* 626:110–116
24. Khuong Ong K, Bai P, Blaha, Wu P (2017) Electronic structure and optical properties of $AFeO_2$ ($A = Ag, Cu$) within GGA calculations. *Chem Mater* 19:634–640
 25. Riveros G, Garin C, Ramírez D, Dalchiele EA, Marotti RE, Pereyra CJ, Spera E, Gómez H, Grez P, Martín F, Ramos-Barrado JR (2015) Delafossite $CuFeO_2$ thin films electrochemically grown from a DMSO based solution. *Electrochim Acta* 164:297–306
 26. Prevot Mathieu S, Jeanbourquin Xavier A, Bourée Wiktor S, Abdi Fatwa, Friedrich Dennis, van de Krol Roel, Guijarro Néstor, Le Formal Florian, Sivula Kevin (2015) Enhancing the performance of a robust sol–gel-processed p-type Delafossite $CuFeO_2$ photocathode for solar water reduction. *Chemsuschem* 8:1359–1367
 27. Zhu T, Deng Z, Fang X, Dong W, Shao J, Tao R, Wang S (2016) Room temperature deposition of amorphous p-type $CuFeO_2$ and fabrication of $CuFeO_2/n$ -Si heterojunction by RF sputtering method. *Bull Mater Sci* 39(3):883–887
 28. Bera A, Deb K, Sinthika S, Thapa R, Saha B (2018) Chemical modulation of valence band in delafossite structured $CuFeO_2$ thin film and its photoresponse. *Mater Res Express* 5:015909
 29. Chen Hong-Ying, Fu Guan-Wei (2014) Influences of post-annealing conditions on the formation of delafossite- $CuFeO_2$ thin films. *Appl Surf Sci* 288:258–264
 30. Deng Z, Fang X, Wang X, Wu S, Dong W, Shao J, Tao R (2015) Characterization of amorphous p-type transparent $CuFeO_2$ thin films prepared by radio frequency magnetron sputtering method at room temperature. *Thin Solid Films* 589:17–21
 31. Abdelwahab HM, Ratep A, Abo Elsoud M, Boshta M, Osman MBS (2018) Influences of annealing temperature on sprayed $CuFeO_2$ thin films. *Results Phys* 9:1112–1115
 32. Chen H-Y, Wu J-H (2012) Characterization and optoelectronic properties of sol–gel-derived $CuFeO_2$ thin films. *Thin Solid Films* 520:5029–5035
 33. Alkhayatt AHO, Thahab SM, Zgair IA (2016) Structure, surface morphology and optical properties of post-annealed delafossite $CuFeO_2$ thin films. *Optik* 127:3745–3749
 34. Lalanne M, Barnabe A, Mathieu F, Tailhades Ph (2019) Synthesis and thermostructural studies of a $CuFe_{1-x}Cr_xO_2$ delafossite solid solution with $0 \leq x \leq 1$. *Inorg Chem* 48:6065–6071
 35. Zheng SY, Jiang GS, Su JR, Zhu CF (2006) The structural and electrical property of $CuCr_{1-x}Ni_xO_2$ delafossite compounds. *Mater Lett* 60:3871–3873
 36. Lim SH, Desu S, Rastogi AC (2008) Chemical spray pyrolysis deposition and characterization of p-type $CuCr_{1-x}Mg_xO_2$ transparent oxide semiconductor thin films. *J Phys Chem Solids* 69:2047–2056
 37. Lekse JW, Underwood MK, Lewis JP, Matranga C (2012) Synthesis, characterization, electronic structure, and photocatalytic behavior of $CuGaO_2$ and $CuGa_{1-x}Fe_xO_2$ ($x = 0.05, 0.10, 0.15, 0.20$) delafossites. *J Phys Chem C* 116:1865–1872
 38. Lee M, Kim D, Yoon YT, Kim YI (2014) Photoelectrochemical water splitting on a delafossite $CuGaO_2$ semiconductor electrode. *Bull Korean Chem Soc* 35(11):3261–3266
 39. Salke NP, Kamali K, Ravindran TR, Balakrishnan G, Rao R (2015) Raman spectroscopic studies of $CuFeO_2$ at high pressures. *Vib Spectrosc* 81:112–118
 40. Aktas O, Truong KD, Otani T, Balakrishnan G, Clouter MJ, Kimura T, Quirion G (2012) Raman scattering study of delafossite magnetoelectric multiferroic compounds: $CuFeO_2$ and $CuCrO_2$. *J Phys: Condens Matter* 24:036003
 41. van der Pauw LJ (1958) A method of measuring the resistivity and hall coefficient of lamellae of arbitrary shape. *Philips Res Rept* 13:1–9
 42. Tauc J (1968) Optical properties and electronic structure of amorphous Ge and Si. *Mater Res Bull* 3:37–46
 43. Pankove JI (1971) Optical processes in semiconductors. Prentice Hall, Upper Saddle River
 44. Tauc J (1972) In: Abeles F (ed) Optical properties of solids. North-Holland, Amsterdam, p 227
 45. Nie X, Wei S, Zhang SB (2002) Bipolar doping and band-gap anomalies in delafossite transparent conductive oxides. *Phys Rev Lett* 88:066405
 46. Collaboration: Authors and editors of the volumes III/17B-22A-41B (1999) Cadmium sulfide (CdS) band structure, energy gap, cubic modification. In: Madelung O, Rössler U, Schulz M (eds) II-VI and I-VII compounds; semimagnetic compounds. Landolt-Börnstein—Group III Condensed Matter (Numerical Data and Functional Relationships in Science and Technology), vol 41B. Springer, Berlin
 47. Nawle Anant C, Humbe Ashok V, Babrekar MK, Deshmukh SS, Jadhav KM (2017) Deposition, characterization, magnetic and optical properties of Zn doped $CuFe_2O_4$ thin films. *J Alloys Compd* 695:1573–1582
 48. (2009) Physics of semiconductor devices. Lecture 35: photoconductivity, NPTEL. A project funded by MHRD, Govt. of India <https://nptel.ac.in/about.php>. Accessed Nov 2018
 49. Prevot Mathieu S, Jeanbourquin Xavier A, Bouree Wiktor S, Abdi Fatwa, Friedrich Dennis, van de Krol Roel, Guijarro Nestor, Le Formal Florian, Sivula Kevin (2017) Evaluating charge carrier transport and surface states in $CuFeO_2$ photocathodes. *Chem Mater* 29:4952–4962

Publisher's Note Springer Nature remains neutral with regard to jurisdictional claims in published maps and institutional affiliations.